J Fluoresc (2011) 21:545–554
DOI 10.1007/s10895-010-0741-y

ORIGINAL PAPER

A Comprehensive Investigation on the Cooperative Branch Effect on the Optical Properties of Novel Conjugated Compounds

Long Yang · Fang Gao · Jian Liu · Xiaolin Zhong · Hongru Li · Shengtao Zhang

Received: 11 April 2010 / Accepted: 29 September 2010 / Published online: 6 October 2010
© Springer Science+Business Media, LLC 2010

Abstract This paper presents a variety of conjugated derivatives with different number of arms (4-styryl-triphenylamine: **C1**, 4, 4′-di-styryltriphenylamine: **C2,** 4, 4′, 4″-tri-styryltriphenylamine: **C3**). The linear absorption and fluorescence maxima and the molar extinction coefficients are in the order of **C1**<**C2**<**C3** in various solvents. Two-photon absorption (TPA) up-converted emission of the derivatives were determined with Ti: sapphire femtosecond laser. The maximal TPA emission wavelength and the two-photon absorption cross section of the derivatives are also in the order of **C1**<**C2**<**C3** in various solvents. The dipole moment changes of the derivatives between the excited state and the ground state were estimated from experiment, and they are in the order of **C1**<**C2**<**C3**, which is confirmed further by the molecular geometry optimization of the derivatives. The electron density distribution and the energy levels of the frontier orbital of the derivatives were analyzed. The cyclic voltammograms of the derivatives were performed and discussed.

Keywords Synthesis · Optical properties · Molecular geometry optimization · Branch effect · Conjugation

Introduction

In recent years, one of the central themes in organic and material chemistry is to develop highly fluorescent and two-photon absorption (TPA) dyes due to their wide applications such as two-photon fluorescence sensors [1, 2], two-photon biomarkers [3, 4], two-photon imaging reagents [5, 6], two-photon photodynamic therapy [7, 8] and non-linear optical materials [9, 10]. An ideal dye should have excellent spectral characteristics such as high fluorescence quantum yield, large molar extinction coefficient and remarkable TPA cross section in the red-NIR range (700–1200 nm), hence this could guarantee the use of lower concentrations of the sample in applications, which stimulates the development of new two-photon compounds with large TPA cross sections [11–18], which normally have typical phenylvinyl chemical structures with donor-π-donor, donor-π-acceptor and donor-acceptor-donor characteristics.

Many branched compounds containing various electron-donating or accepting groups in the conjugated arms were reported, and the optical characteristics were found to be related to the molecular structures [19, 20]. While to date, the branched conjugated two-photon dyes without push-pull groups have not been explored well. It is surprise because such molecules could show clearly branch effect on the optical properties of the armed derivatives. Such investigation is very necessary because the results could help us on the development of novel optical materials. Consequently, we develop new fluorescent derivatives containing only core and phenyl ring, which means that no electron-donating or accepting groups are located in the arms of the derivatives, thus the substituent effect could be eliminated. This paper presents the synthesis of 4-styryl-triphenylamine (**C1**), 4, 4′-di-styryl–triphenylamine (**C2**) and 4, 4′, 4″-tri-styryl–triphenylamine (**C3**) (Fig. 1)**.** Of its particular interest is trying to investigate pure branch effect on the optical properties (one- and two- photon). The molecular geometry optimization and the electrochemistry of the derivatives were studied to reveal further the deep reasons for the different optical properties.

L. Yang · F. Gao (✉) · J. Liu · X. Zhong · H. Li (✉) · S. Zhang
College of Chemistry and Chemical Engineering,
Chongqing University,
Chongqing 400044, China
e-mail: fanggao1971@gmail.com
e-mail: hongruli1972@gmail.com

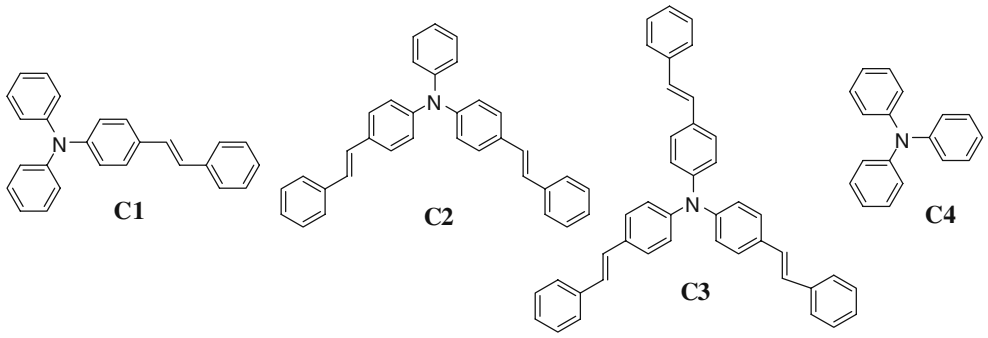

Fig. 1 Chemical structures of the derivatives studied in this paper

Experimental

Reagents and Materials

Organic solvents were obtained from Chongqing Medical and Chemical Corporation. Other chemicals and reagents were purchased from Aldrich unless otherwise specified. The organic solvents were dried using standard laboratory techniques according to the published methods [21]. The starting materials were further purified with redistillation or recrystallization before use. The derivatives **C1** to **C3** (Fig. 1) were synthesized in our laboratory, and **C2** and **C3** were firstly reported.

Instruments

The UV/visible absorption spectra (1×10^{-5} mol/L) were recorded with a Cintra spectrophotometer. The emission spectra (1×10^{-5} mol/L) were checked with Shimadzu RF-531PC spectrofluorophotonmeter. Rodamin 6G in ethanol (Φ=0.94, 1×10^{-6}–1×10^{-5} mol/L) was used as reference to determine the fluorescence quantum yields of the compounds herein [22, 23]**.** To avoid self-quenching of fluorescence emission, the low concentration of the compounds (1×10^{-6} mol/L) was prepared for the survey of fluorescence quantum yields. The melting point was determined using a Beijing Fukai melting point apparatus. Nuclear magnetic resonance (NMR) spectroscopy was conducted at room temperature on a Bruker 500 MHz apparatus with tetramethylsilane (TMS) as an internal standard and $CDCl_3$ as solvent. Elemental analysis was performed by a CE440 elemental analysis meter from Exeter Analytical Inc.

The fluorescence quantum yields of the compounds in solvents with different polarities were measured based on the following equation [24, 25]:

$$\Phi_f = \Phi_f^0 \frac{n_0^2 A^0 \int I_f(\lambda_f) d\lambda_f}{n^2 A \int I_f^0(\lambda_f) d\lambda_f} \quad (1)$$

wherein $\boldsymbol{n^0}$ and $\boldsymbol{n}$ are the refractive indices of the solvents, $\boldsymbol{A^0}$ and $\boldsymbol{A}$ are the optical densities at excitation wavelength, $\boldsymbol{\Phi_f}$ and $\boldsymbol{\Phi_f^0}$ are the quantum yields, and the integrals denote the area of the fluorescence bands for the reference and sample, respectively.

Two-photon excited fluorescence spectra, pumped by Ti: sapphire femto-second laser (Spectra-Physics Ltd., Tsunami mode-locked, 80 MHz, <130 f s, average power ≤700 mW) tuned by step of 20 nm in the range of 700~880 nm, were recorded on Ocean Optics USB2000 CCD camera with detecting range of 180~880 nm. TPA cross-section (σ) was determined by up-conversion fluorescence method using 5×10^{-4} mol/L fluorescein in 0.1 mol/L solution of NaOH as reference sample [26]. The sample was bubbled with nitrogen for 15 min to eliminate oxygen before the detection. TPA cross sections of the compounds were determined by the following equations [27]:

$$\sigma = \frac{\sigma^{TPE}}{\Phi_F} \quad (2)$$

$$\sigma^{TPE} = \sigma_{cal}^{TPE} \frac{c_{cal}}{c} \frac{n_{cal}}{n} \frac{S}{S_{cal}} \quad (3)$$

Wherein $\boldsymbol{\sigma}$ is two-photon absorption section, $\boldsymbol{\sigma^{TPE}}$ is two-photon excited crossing section, $\boldsymbol{c}$ is the concentration of reference and sample molecules, $\boldsymbol{n}$ is refractive index of the solvent, and $\boldsymbol{S}$ is two-photon up-conversion fluorescence intensity, ***cal*** represents as reference.

Molecular Geometry Optimization

Molecular geometry optimization was conducted with the HyperChem 8.0 package [28] via AM1 semi-empirical quantum chemical method to keep the computations tractable [29].

Cyclic Voltammograms

Cyclic voltammograms was carried out using a Shanghai Chenhua electrochemical working station. Two Pt work electrodes and an Ag/Ag^+ reference electrode, namely three electrodes system, were included in cell. Typically, a 0.05 mol/L solution

of tetra-n-butylammonium hexaflorophosphate in CH_2Cl_2 containing of dyes was bubbled with argon for 15 min.

Synthesis

The synthesis of the derivatives was depicted in Scheme 1. 4-Formyl-triphenylamine and 4′,4″-diformyl-triphenylamine, 4′,4″,4‴—triformyl-triphenylamine were prepared according to well-known procedures with modified procedure respectively [30]. Benzyl bromide (17.5 mmol, 3.00 g) reacted with triethyl phosphite (10 ml) under 130–160 °C for 6 h. After excess triethyl phosphite was removed in vacuum, the crude benzyl-phosphonate was obtained, which directly went to the next step without further purification.

(1) *C1: 4-styryl-triphenylamine*

Benzylphosphonate (8.77 mmol, 2.00 g) reacted with 4-formyl-triphenylamine (7.31 mmol, 2.00 g) in 50 ml dry tetrahydronfuran using sodium methoxide (17.5 mmol, 0.98 g) as base at room temperature overnight. After the filtration of solid materials and the evaporation of solvent in vacuum, the reactant mixture was dissolved in chloroform and washed by water. The organic layer was dried with

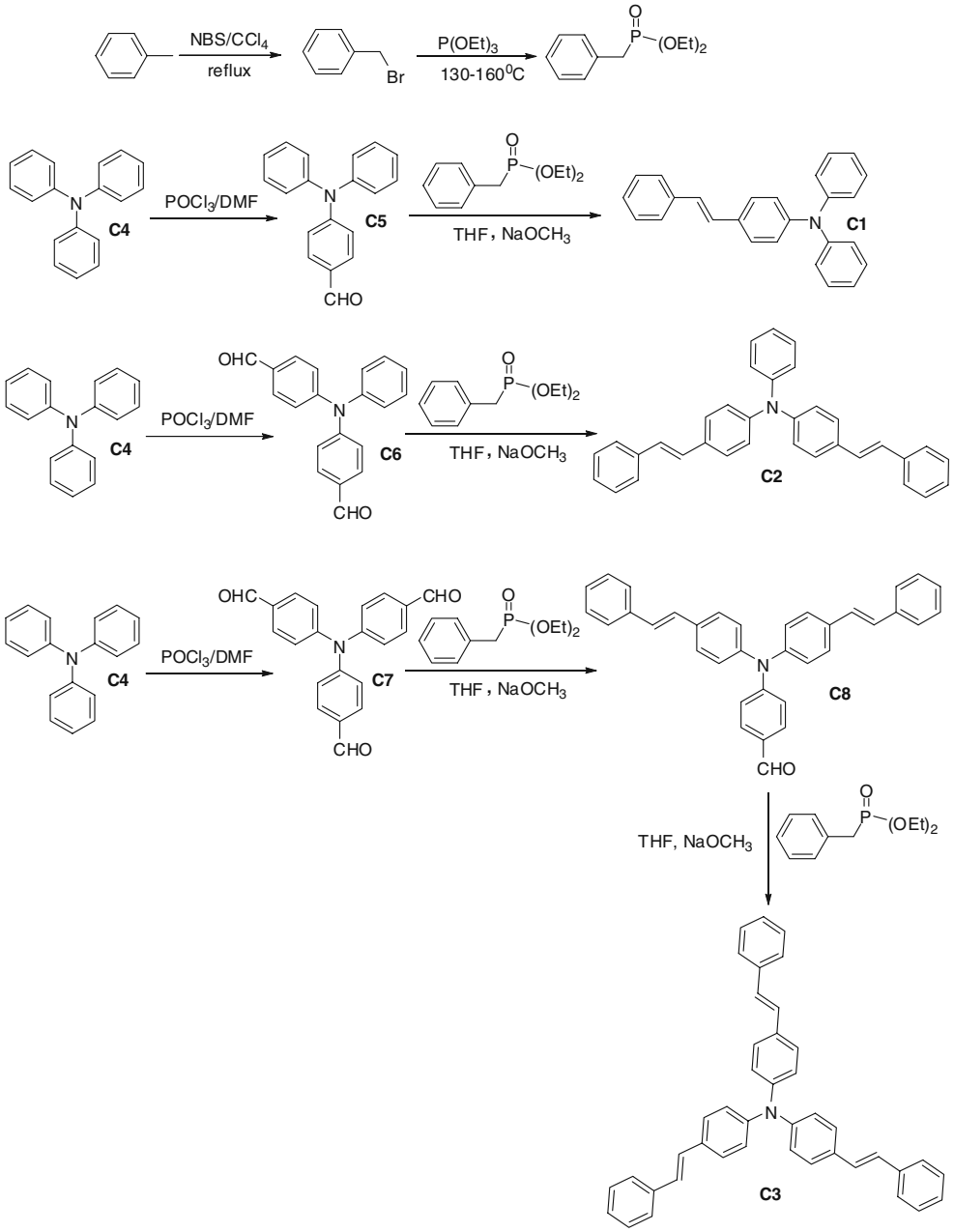

Scheme 1 Synthesis routes of C1, C2 and C3

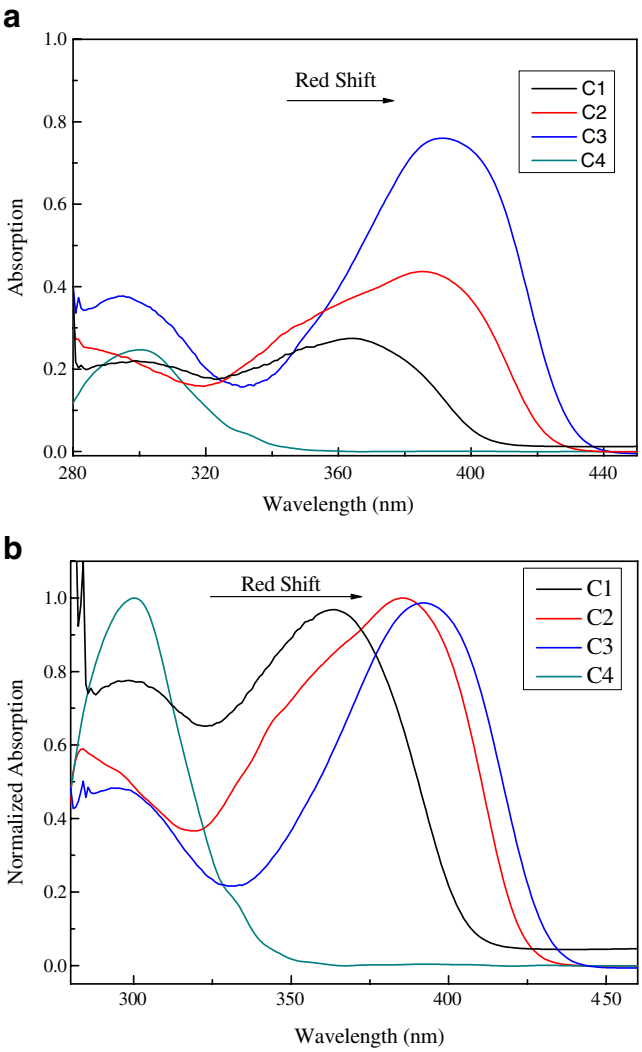

Fig. 2 Typical UV/visible absorption spectroscopy of **C1** to **C4** in benzene (c: 1×10^{-5} mol/L) **a** Real spectroscopy, **b** Normalized Spectroscopy

anhydrous magnesium sulphate. After evaporated in vacuum, **C1** was purified with column chromatography using benzene as eluent, which was further purified with recrystallization in cyclohexane. **C1**: color: yellow, yield: 60%, m.p.: 141–142 °C, ^{1}H-NMR ($CDCl_3$, 500 MHz) δ(ppm): 7.532–7.548(d, 2H, *J*=8.0 Hz, Ar-H), 7.428–7.448 (d, 2H, *J*=10.0 Hz, Ar-H), 7.377–7.412 (t, 2H, *J*=7.75 Hz, Ar-H), 7.283–7.325 (m, 4H, Ar-H), 7.269 (s, 1H, Ar-H), 7.156–7.172 (d, 2H, *J*=8.0 Hz, Ar-CH = CH), 7.129 (s, 2H, Ar-H), 7.029–7.118(m, 6H, Ar-H). ^{13}C-NMR ($CDCl_3$, 125 MHz): 123.077, 123.658, 124.534, 126.368, 127.335, 127.417, 128.230, 128.710, 129.340, 137.679, 147.411, 147.610. Anal. Calcd (Found) for $C_{26}H_{21}N$ (%): C, 89.81 (89.89), H, 6.15 (6.09), N, 4.06 (4.01).

(2) *C2: 4,4′-di- styryl -triphenylamine*

Benzylphosphonate (8.77 mmol, 2.00 g) reacted with 4,4′-diformyl-triphenylamine (3.65 mmol, 1.10 g,) in 60 ml dry tetrahydronfuran using sodium methoxide (17.5 mmol, 0.98 g) as base at room temperature overnight. After the filtration of solid materials and the evaporation of solvents in vacuum, the reactant mixture was dissolved in chloroform and washed by water. The organic layer was dried with anhydrous magnesium sulphate. After evaporated in vacuum, **C2** was purified with column chromatography using benzene as eluent, which was further purified with recrystallization in cyclohexane. **C2**: color: yellow, yield: 40%, m.p.: 152–153 °C. ^{1}H-NMR($CDCl_3$, 500 MHz) δ(ppm): 7.487–7.504 (d, 4H, *J*=8.5 Hz, Ar-H), 7.390–7.415 (d, 4H, *J*=12.5 Hz, Ar-H), 7.330–7.361 (t, 4H, *J*= 7.7 Hz, Ar-H), 7.223–7.293 (m, 5H, Ar-H), 7.127–7.147 (d, 2H, *J*=10.0 Hz, Ar-H), 7.072–7.094 (d, 4H, *J*=11.0 Hz, Ar-H), 7.025–7.076 (t, 4H, *J*=12.7 Hz, Ar-H), ^{13}C-NMR ($CDCl_3$, 125 MHz): 123.363, 123.975, 124.763, 126.353, 127.273, 127.352, 127.430, 128.129, 128.686, 129.379, 131.901, 137.605, 147.039, 147.039. Anal. Calcd (Found) for $C_{34}H_{27}N$ (%): C, 90.90 (90.87), H, 6.01 (6.13), N, 3.13 (3.09).

(3) *C3: 4,4′,4″-tri- styryl -triphenylamine*

Benzylphosphonate (8.77 mmol, 2.00 g) reacted with 4,4′,4″-triformyl-triphenylamine (2.92 mmol, 0.96 g,) in 60 ml dry tetrahydronfuran using sodium methoxide (17.5 mmol, 0.98 g) as base at room temperature overnight. After the filtration of solid materials and the evaporation of solvents in vacuum, the reactant mixture was dissolved in chloroform and washed by water. The organic layer was

Table 1 Maximal absorption wavelength ($\lambda_{a,max}$, nm) and the molar extinction coefficients (ε) of the derivatives

Compounds		Solvents				
		Benzene	THF	EtOAc	CH_2Cl_2	CH_3CN
C1	$10^{-5}\varepsilon$	0.279	0.339	0.320	0.364	0.322
	$\lambda_{a,max}$	363	364	358	366	358
C2	$10^{-5}\varepsilon$	0.430	0.435	0.437	0.439	0.451
	$\lambda_{a,max}$	384	382	379	385	379
C3	$10^{-5}\varepsilon$	0.760	0.970	0.689	0.750	0.715
	$\lambda_{a,max}$	390	388	386	390	387

ε: $mol^{-1}\cdot lcm^{-1}$

dried with anhydrous magnesium sulphate. After evaporated in vacuum, the crude 4-formyl-4′,4″-di-styryl–triphenylamine (**C8**) was purified with column chromatography using benzene as eluent, which was further purified with recrystallization in cyclohexane. **C8**: color: yellow, yield: 52%, m.p., 94–95 °C. ^{1}H-NMR ($CDCl_3$,500 MHz) δ(ppm): 7.696–7.723(d, 2H, *J*=13.5 Hz, Ar-*CHO*), 7.494–7.515(d, 4H, *J*=10.5 Hz, Ar-H), 7.466–7.488(d, 4H, *J*=11.0 Hz, Ar-H), 7.342–7.373(t, 4H, *J*=7.75 Hz, Ar-H), 7.245–7.274(t, 2H, *J*=7.25 Hz ,Ar-*H*), 7.139–7.165(d, 4H, *J*=13.0 Hz, Ar-CH = CH), 7.043–7.116(t, 6H, *J*=18.3 Hz, Ar-H).

Benzylphosphonate (8.77 mmol, 2.00 g) reacted with 4-formyl-4′,4″-di-styryl –triphenylamine (**C8**) (7.31 mmol, 3.49 g) in 60 ml dry tetrahydronfuran using sodium methoxide (17.5 mmol, 0.98 g) as base at room temperature overnight. The reactant mixture was processed in the same procedure as **C2** to obtain **C3**. **C3**: color: yellow, yield: 35%, m.p. >300 °C. ^{1}H-NMR ($CDCl_3$,500 MHz) δ(ppm): 7.507–7.522(d, 6H, *J*=7.5 Hz, Ar-*H*), 7.426–443 (d, 6H, *J*=8.5 Hz, Ar-H), 7.348–7.379(t, 6H, *J*=7.8 Hz, Ar-H), 7.242–7.271(t, 3H, *J*=7.3 Hz, Ar-H), 7.109–7.131 (d, 6H, Ar-*CH* = *CH*), 7.020–7.077(t, 6H, *J*=14.3 Hz, Ar-H). ^{13}C-NMR ($CDCl_3$, 125 MHz): 124.9, 126.9, 127.4, 127.9, 128.5, 128.6, 129.7,137.5, 145.1. Anal. Calcd (Found) for $C_{30}H_{27}NO_4$ (%), C, 91.13 (91.24), H, 6.13 (6.01), N, 2.74 (2.67).

Results and Discussion

Linear Optical Properties

A typical UV/visible absorption spectroscopy of **C1** to **C3** in benzene is presented in Fig. 2. The derivatives exhibit double absorption peaks from 275 to 550 nm. The first absorption peaks of the derivatives are similar to the absorption spectroscopy of triphenylamine, indicating that it could be from the local electron transition of triphenyl-

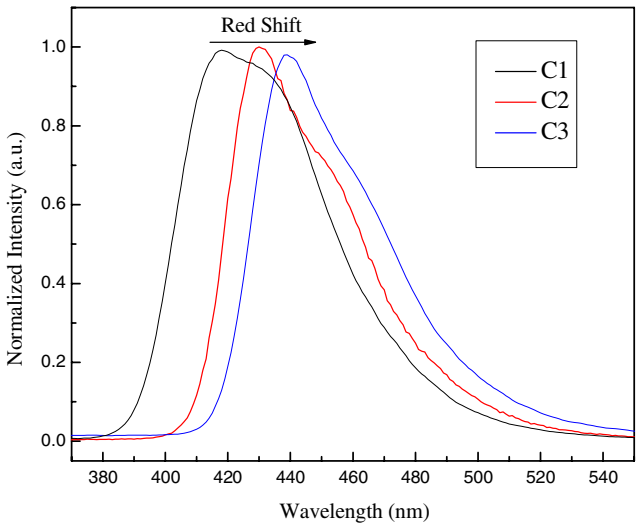

Fig. 3 Normalized fluorescence spectroscopy of **C1**, **C2** and **C3** in benzene

Table 2 Maximal linear emission wavelength ($\lambda_{f,max}$, nm) and the quantum yields of **C1** to **C3**

Compounds		Solvents				
		Benzene	THF	EtOAc	CH_2Cl_2	CH_3CN
C1	ϕ	0.75	0.96	0.89	0.97	0.88
	$\lambda_{f,max}$	421	436	434	443	456
C2	ϕ	0.86	0.80	0.76	0.69	0.39
	$\lambda_{f,max}$	432	446	442	456	473
C3	ϕ	0.67	0.57	0.60	0.55	0.51
	$\lambda_{f,max}$	441	467	462	473	483

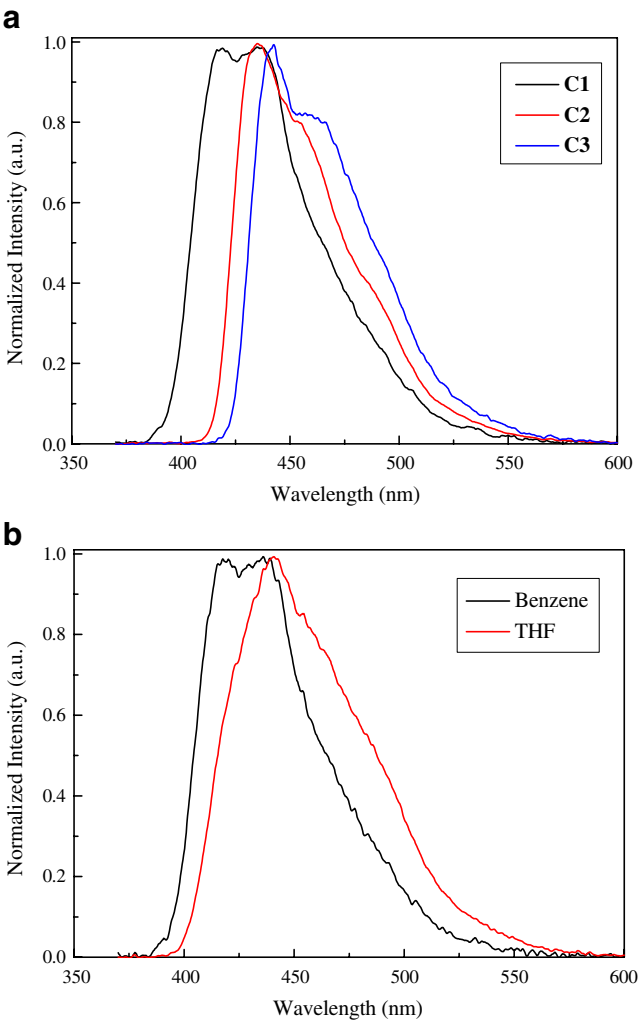

Fig. 4 Two-photon induced up-conversion fluorescence emission of the derivatives in solvents excited by 700 nm Ti: sapphire laser **a C1**, **C2**, **C3** in benzene; **b C1** in benzene and THF

Table 3 Two-photon optical data of **C1** to **C3** in 700 nm laser frequency

Solvents	C1		C2		C3	
	λ_{max} (TPA)	σ_{TPA}/GM	λ_{max} (TPA)	σ_{TPA}/GM	λ_{max} (TPA)	σ_{TPA}/GM
Benzene	418	46.6	436	218.6	443	254.0
THF	441	57.6	462	290.7	479	288.0

λ_{max} (TPA): nm, the maximal up-conversion fluorescence wavelength, σ: two-photon crossing section (GM, $1GM=10^{-50}$ cm·s·photo^{-1})

amine core. The second absorption peaks of the derivatives, namely the maximal absorption peak, could be ascribed to the (π, π*) transition [31]. The absorption spectral data of **C1** to **C3** in various solvents were listed in Table 1. The data show that the maximal absorption wavelength displays gradual red-shift in the order of **C1**<**C2**<**C3**. This suggests that the extent of internal charge transfer is related to the number of branches. The maximal absorption wavelength of the derivatives exhibits some bathochromic shift with the increasing of solvent polarity, which is due to internal charge transfer nature of (π, π*) electron transition of the derivatives [32]. Interesting, the molar extinction coefficients of the derivatives increase with the number of arms. Table 1 shows that the ratio of the molar extinction coefficients of **C1**, **C2** and **C3** is close to the ratio of the number of arms, namely 1:2:3. It could be easily understood from their chemical features. **C1**, **C2** and **C3** are characterized with D-π, D-(π)2, D-(π)3 respectively, which results in a cooperative effect of the molar extinction coefficients of the derivatives**.** Figure 3 shows a gradual red-shift for the maximal fluorescence wavelength as **C1**<**C2**<**C3**. This indicates that the order of the extent of internal charge transfer in the excited state is **C1**<**C2**<**C3**. The fluorescence quantum yields and the maximal linear emission wavelength of the derivatives are presented in Table 2. The data show that **C1**, **C2** and **C3** exhibit strong fluorescence in various solvents. The emission maxima of the derivatives shift to long wavelength in polar solvents. This means that the fluorescence spectroscopy displays more remarkable solvent effect than the absorption spectroscopy, which implies that a large internal charge transfer occurs in the excited state.

Two-Photon Optical Properties

We observed that TPA fluorescence of the derivatives was quenched at high concentration solution, thus 5×10^{-4} mol/L sample solution was used for the TPA determination. The derivatives display remarkable TPA emission in 700 nm Ti:sapphire femto-second laser excitation. Figure 4(a) presents TPA emission of these compounds under 700 nm laser in benzene**.** Clearly, the maximal TPA emission exhibit gradual red-shift in the order of **C1**→**C2**→**C3**. Figure 4 (b) shows the TPA fluorescence of **C1** in benzene and tetrahydrofuran (THF) at 700 nm. Obviously, the maximal TPA emission of **C1** exhibits red-shift with the increasing

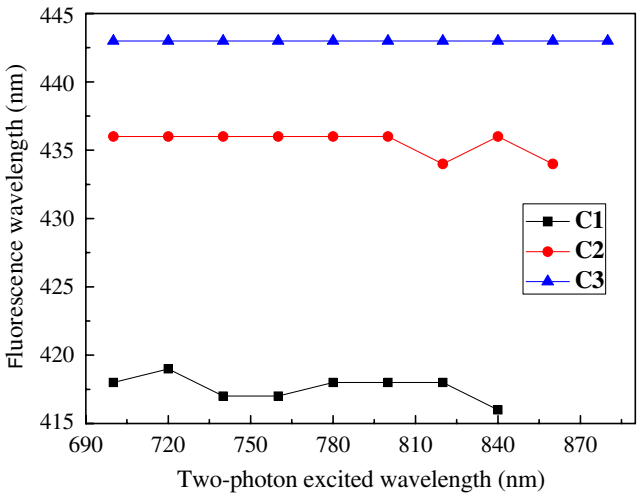

Fig. 5 Maximal TPA emission wavelengths of the derivatives in benzene excited by different laser frequencies

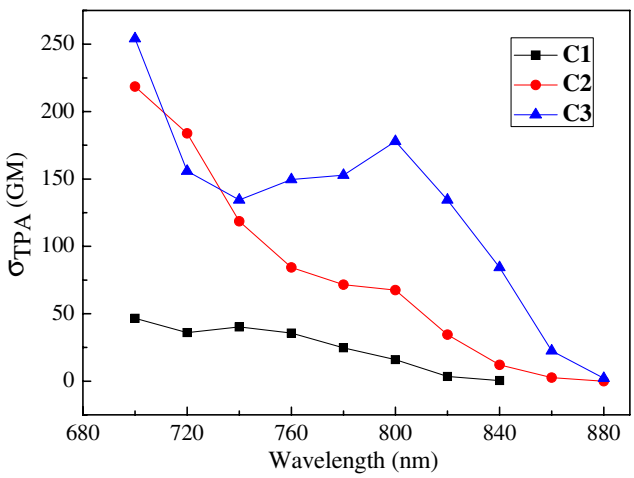

Fig. 6 TPA cross-sections (σ_{TPA}) of **C1**, **C2** and **C3** in benzene in various laser frequencies from 700 nm to 880 nm (c: 5×10^{-4} mol/L)

polarity of the solvents. Table 3 presents the maximal TPA emission and TPA cross sections of the derivatives. The results show that the orders of the maximal TPA emission wavelength and TPA cross sections of the derivatives are the same (**C3>C2>C1**), reflecting a cooperative branch effect on two-photon optical properties. TPA cross sections of the derivatives become larger with the increasing polarity of the solvents, which could be ascribed to larger dipole moment changes between the excited state and the ground state caused by stronger intramolecular charge transfer in polar solvents. It is well accepted that the larger dipole moment changes between the ground state and the excited state lead to not only the red-shift of the maximal TPA emission, but the larger TPA cross section [33–35].

We also utilized different excited wavelength (700~880 nm) to detect TPA fluorescence of the derivatives. The maximal TPA emission wavelengths of the derivatives excited by different laser frequencies are presented in Fig. 5. It is interesting to observe that the maximal TPA emission of **C1** is independence on the excited wavelength and it is almost identical to one-photon maximal fluorescence wavelength, which implies that one-photon and two-photon excited fluorescence spectroscopy could be from the same or similar excited state. Figure 6 shows the TPA cross sections of the derivatives in various laser frequencies. Clearly, the TPA cross sections are in the order **C3>C2>C1** in most laser frequencies, which reveals further the branch cooperative effects on the two-photon optical properties. We shall point out that the TPA cross section of **C1** is very close to reported data [36]. Herein, the relationship of TPA intensities of the he derivatives and the pumped powers were determined further, which follows well the square law in the 800 nm laser excitation (Fig. 7), and the slopes of 1.916 and 1.973 for **C2** and **C3** respectively demonstrate that the derivatives have excellent two-photon absorption nature [26].

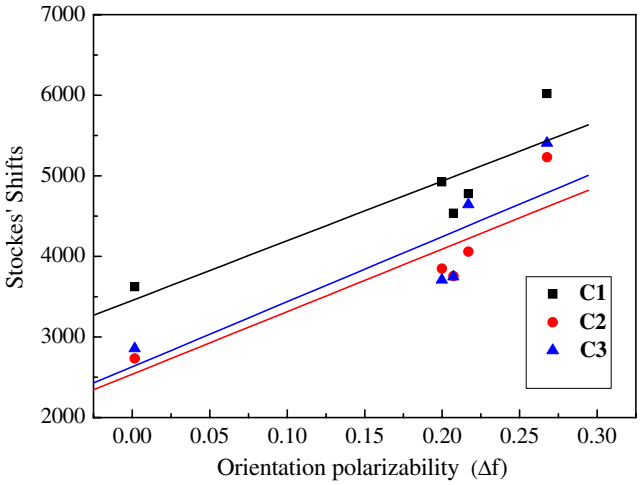

Fig. 8 Relationship between Stokes' shifts of the derivatives and the orientation polarizability (Δf) of solvents respectively

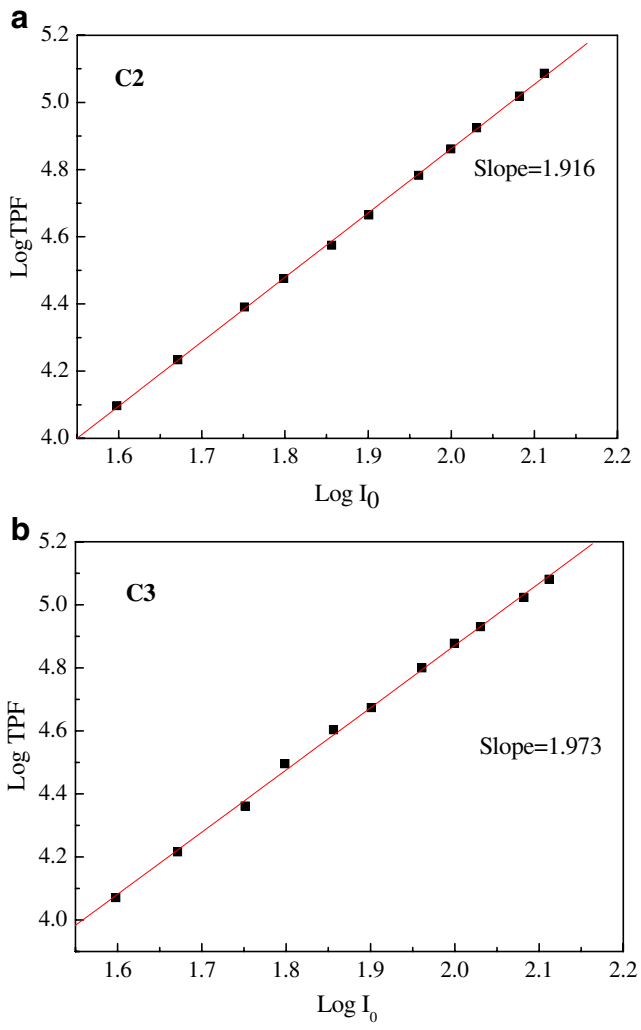

Fig. 7 Square relationships between TPF (TPA fluorescence) intensity of the derivatives and the excited laser powers at 800 nm **a** for **C2**, **b** for **C3**

Dipole Moment Changes

It is well accepted that the dipole moment changes are related with the optical properties of organic compounds.

Table 4 Changes of dipole moment between the excited state and ground state respectively obtained from experiments and theoretical calculations

Dipole moments change Δμ (Derby)	C1	C2	C3
From experiment	2.59	3.92	4.01
From theory*	2.76	2.87	3.05

1 $D=3.336\times10^{-30}$ c.m, * in vacuum, for single molecule

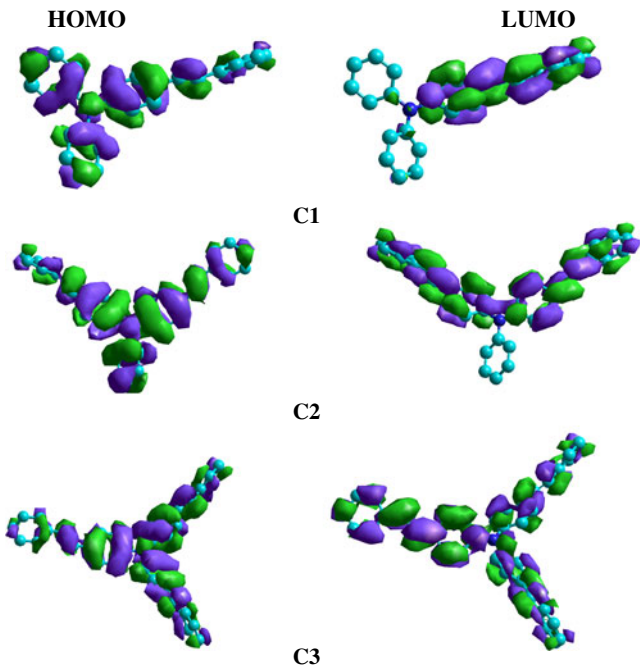

Fig. 9 Electron density distributions of frontier orbital of **C1**, **C2** and **C3**

We further estimated the dipole moment changes between the excited state and the ground state based on Lippert equation [37, 38]:

$$hc(\nu_{abs} - \nu_{em}) = \frac{2\left(\mu_e - \mu_g\right)^2}{4\pi\varepsilon_0 a^3}\Delta f + const \quad (4)$$

$$\Delta f = \left(\frac{\varepsilon - 1}{2\varepsilon + 1} - \frac{n^2 - 1}{2n^2 + 1}\right) \quad (5)$$

Wherein $\boldsymbol{h}$ is Planck's constant, $\boldsymbol{c}$ is the speed of light, and $\boldsymbol{\Delta f}$ is called the orientation polarizability. $\boldsymbol{\upsilon_{abs}}$, $\boldsymbol{\upsilon_{em}}$ are the wavenumbers of the absorption and emission respectively, $\boldsymbol{n}$ is the refractive index, and $\boldsymbol{\varepsilon}$ is the relative low-frequency dielectric constant of the solvents. The chromophore group is considered as a dipole, which locates in a cavity with a radius of $\boldsymbol{a}$ in a continuous solvent-dipole environment, and Lippert equation describes a solvent effect of the index of refraction and relative dielicetric constant. As a consequence, the linear correlation between Stokes shifts and $\boldsymbol{\Delta f}$ does not reflect some special interaction between the fluorophore and solvent molecules such as hydrogen bonding.

Plots of Stokes shift as a function of the solvent orientation polarizability ($\boldsymbol{\Delta f}$) are shown in Fig. 8. The linear correlations between Stokes shift and orientational polarizability reflects the dipolar solvent effects. The equations are obtained as: **C1**, Y=7402.6X+3454.2, **C2**, Y=7760.3X+2538.1, **C3,** Y=8069.3X+2630.3. Thus, the dipole moment changes between the excited state and the ground state are calculated from the slopes and listed in Table 4. The order of the dipole moment change are **C3**>**C2**>**C1**, which demonstrates that the extent of internal charge transfer in the excited state is greatly influenced by the number of arms. The dipole moment changes between the excited state and ground state were further calculated theoretically on the basis of molecular geometry optimization. Table 4 shows that the theoretical results are good agreement with the experimental results.

As shown in Fig. 9, the derivatives have typical (π, π^*) character, while they exhibit different electron distribution in frontier orbitals. Seen from Fig. 9, for the HOMO orbitals of the derivatives, the electron density is mainly distributed around N-core. While for the LUMO orbital of the derivatives, the majority of the electron density distribution is located at diphenylehylene part. Thus, it is obvious that the majority of the electron density distribution

Table 5 Energy gaps of HOMO and LUMO of the derivatives obtained from theoretical calculations

Derivatives	E_{HOMO} (eV)	E_{LUMO} (eV)	Energy gap (eV)
C1	−7.861	−0.4531	7.4079
C2	−7.793	−0.5585	7.2345
C3	−7.744	−0.5782	7.1658

Table 6 The redox potentials of compounds **C1** to **C3** determined in methylene chloride at 0.1 V·s^{-1}scan rate

Compounds	Oxidation potentials (V)	Reduction potentials (V)
C1	1.11/0.90	0.53/−0.13
C2	1.14/0.72/0.34	0.74/0.49/−0.17
C3	1.16	0.71/−0.14/−0.80
C4	1.03	0.42/−0.26/−0.57

Table 7 Estimated HOMO and LUMO energies of compounds **1** to **3** from cyclic voltammograms

Compounds	λ_{onset} (nm)	Eg (eV)	E_{LUMO} (eV)	E_{HOMO} (eV)
C1	408.0	3.04	−5.45	−8.49
C2	424.8	2.92	−5.48	−8.40
C3	431.2	2.88	−5.50	−8.38

E_g=1240/λ, LUMO(eV) = $-E^{OX}$ −4.34 [41, 42], HOMO(eV) = LUMO–E_g , λ_{onset}:the longest absorption wavelength at ten percent of the maximal UV peak

for **C1** is in one arm in LUMO, and two arms have the most of electron density distribution in LUMO of **C2,** and the electron density is distributed in three arms in LUMO of **C3**. As a consequence, the charge delocalization of frontier orbitals of the derivatives are in the order of **C3**>**C2**>**C1**. The theoretical HOMO-LUMO energy of the derivatives were further calculated, and the results are listed in Table 5, which shows that the order of HOMO-LUMO gap is **C1**>**C2**>**C3**. The results show that the not only the electron density distribution and the dipole moment changes of the excited state and the ground state could be tuned by the numbers of arms, but the energy gaps of the frontier orbital could be regulated. The results explain the gradual red-shift of absorption and fluorescence spectroscopy of **C1**, **C2** and **C3**. This also interprets why the maximal TPA fluorescence wavelength and TPA cross section of the derivatives are related to the number of arms.

Cyclic voltammograms of the derivatives were acquired at various scan rates from 50 to 200 $mV{\cdot}s^{-1}$. No corresponding potentials demonstrate that redox processes of the derivatives are characterized with irreversible nature under all sweeping rates. The linear increasing of peak currents with the square root of scan rates indicates that the electron transfer reactions are controlled by the solvent diffusion [39]. Table 6 presents **t**he redox potentials of **C1** to **C4** at $0.1{\cdot}V{\cdot}s^{-1}$scan rate. Obviously, the first oxidation-reduction potentials of **C1** to **C3** could be assigned to N-core. We further estimated HOMO-LUMO gap based on the optical band gap ($\mathbf{E_g}$), which was calculated from the onset of the longest absorption wavelength at ten percent of the maximal UV peak [40], and the results are presented in Table 7. It clearly shows the HOMO energy of the derivatives is in the order of **C3**>**C2**>**C1**, while LUMO energy is the order of **C1**>**C2**>**C3**, HOMO-LUMO gap is tuned efficiently by the number of branches. It interpreters well why one and two-photon optical properties of the derivatives have a close relationship with the number of arms.

Conclusions

This paper describes strong evidences that one- and two-photon optical properties of conjugated derivatives are affected by the number of arms. The molecular geometry optimization demonstrates that the electron density distribution of the frontier orbital and the dipole moment changes are related to the number of branches of derivatives. The theoretical and experimental results reflect that not only the energy level of the frontier orbital could be mediates by the number of arms, but HOMO-LUMO gap could be regulated. These could be the deep reasons of branch effect on the optical properties of the derivatives. The results presents in this article would be great interest in the development of new branched dyes with required one- and two- optical properties.

Acknowledgements The authors appreciate financial support from National Natural Science Foundation of China (Nos. 20776165, 20702065, 20872184). We would thank "the Foundation of Chongqing Science and Technology Commission" (CSTC2008BA4020, CSTC2009BB4216). H. Li thanks "A Foundation for the Author of National Excellent Doctoral Dissertation of PR China (200735)", and thanks supports from the Key Laboratory of Functional Crystals and Laser Technology, TIPC, Chinese Academy of Sciences. We thank Dr. X. Chen for helpful discussion on molecular geometry optimization. We also thank "Innovative Talent Training Project, the Third State of '211 Project, S-09103', Chongqing University.

References

1. Taki M, Wolford JL, O'Halloran TV (2004) Emission ratiometric imaging of intracellular zinc: design of a Benzoxazole fluorescent sensor and its application in two-photon microscopy. J Am Chem Soc 126(3):712–713
2. Farruggia G, Iotti S, Prodi L, Montalti M, Zaccheroni N, Savage PB, Trapani V, Sale P, Wolf FI (2006) 8-hydroxyquinoline derivatives as fluorescent sensors for magnesium in living cells. J Am Chem Soc 128(1):344–350
3. Rice WL, Kaplan DL, Georgakoudi I (2007) Quantitative biorkers of stem cell differentiation based on intrinsic two-photon excited fluorescence. J Biomed Opt 12(6):060504
4. Wu YC, Qu JY (2005) Two-photon autofluorescence spectroscopy and second-harmonic generation of epithelial tissue. Opt Lett 30(22):3045–3047
5. (a) Tokar VP, Losytskyy MY, Ohulchanskyy TY, Kryvorotenko DV, Kovalska VB, Balanda AO, Dmytruk IM, Prokopets VM, Yarmoluk SM, Yashchuk VM(2010) Styryl dyes as two-photon excited fluorescent probes for DNA detection and two-photon laser scanning fluorescence microscopy of living cells. J Fluorescence 10.1007/s10895-010-0630-4, available in web. (b) Liu B, Zhang HL, Liu J, Huang ZL, Zhao YD, Luo QM (2007) Acetylene-substituted two-photon absorbing molecules with rigid elongated Pi-conjugation: synthesis, spectroscopic properties and two-photon fluorescence cell imaging applications. Journal of Fluorescence 17(5): 573–579 (c) Picot A, D'Aléo A, Baldeck PL, Grichine A, Duperray A, Andraud C, Maury O (2008) Long-lived two-photon excited luminescence of water-soluble europium complex: applications in biological imaging using two-photon scanning microscopy. J Am Chem Soc 130 (5):1532–1533
6. Law GL, Wong KL, Man C, Wong WT, Tsao SW, Lam M, Lam P (2008) Emissive terbium probe for multiphoton in vitro cell imaging. J Am Chem Soc 130(12):3714–3715
7. Kim S, Ohulchanskyy TY, Pudavar HE, Pandey RK, Prasad PN (2007) Organically modified silica nanoparticles co-encapsulating photosensitizing drug and aggregation-enhanced two-photon absorbing fluorescent dye aggregates for two-photon photodynamic therapy. J Am Chem Soc 129(9):2669–2675
8. Karotki A, Khurana M, Lepock JR, Wilson BC (2006) Simultaneous two-photon excitation of photofrin in relation to photodynamic therapy. Photochem Photobiol 82(2):443–452
9. Babgi B, Rigamonti L, Cifuentes MP, Corkery TC, Randles MD, Schwich T, Petrie S, Stranger R, Teshome A, Asselberghs I, Clays K, Samoc M, Humphrey MG (2009) Length-dependent convergence and saturation behavior of electrochemical, linear optical, quadratic nonlinear optical, and cubic nonlinear optical properties

of dipolar alkynylruthenium complexes with oligo(phenyleneethynylene) bridges. J Am Chem Soc 131(29):10293–10307
10. Liu CG, Guan W, Yan LK, Su ZM, Song P, Wang EB (2009) Second-order nonlinear optical properties of transition-metal-trisubstituted polyoxometalate–diphosphate complexes: a donor–conjugated bridge–acceptor paradigm for totally inorganic nonlinear optical materials. J Phys Chem C 113(45):19672–19676
11. (a) Reinhardt BA (1998) Highly active two-photon dyes: design, synthesis, and characterization toward application. Chem Mater 10 (7): 1863–1874 (b) Meltola NJ, Vaarno J, Soini AE (2005) Dipyrrylmetheneboron difluorides as labels in two-photon excited fluorometry. Part II–nucleic acid hybridization assays. J Fluorescence 15(3):233–242
12. Belfield KD, Liu Y, Negres RA, Fan M, Pan G, Hagan DJ, Hernandez FE (2002) Two-photon photochromism of an organic material for holographic recording. Chem Mater 14 (9):3663–3667
13. He GS, Dai TC, Lin JM, Prasad PN, Kannan R, Dombroskie AG, Vaia RA, Tan LS (2004) Degenerate two-photon-absorption spectral studies of highly two-photon active organic chromophores. J Chem Phys 120(11):5275–5284
14. Bordeau G, Lartia R, Metge G, Fiorini-Debuisschert C, Charra F, Teulade-Fichou MP (2008) Trinaphthylamines as robust organic materials for two-photon-induced fluorescence. J Am Chem Soc 130(50):16836–16837
15. Williams-Harry M, Bhaskar A, Ramakrishna G, Goodson T, Imamura M, Mawatari A, Nakao K, Enozawa H, Nishinaga T, Iyoda M (2008) Giant thienylene-acetylene-ethylene macrocycles with large two-photon absorption cross section and semishape-persistence. J Am Chem Soc 130(11):3252–3253
16. Beverina L, Crippa M, Landenna M, Ruffo R, Salice P, Silvestri F, Versari S, Villa A, Ciaffoni L, Collini E, Ferrante C, Bradamante S, Mari CM, Bozio R, Pagani GA (2008) Assessment of water-soluble π-extended squaraines as one- and two-photon singlet oxygen photosensitizers: design, synthesis, and characterization. J Am Chem Soc 130(6):1894–1902
17. Pawlicki M, Collins HA, Denning RG, Anderson HL (2009) Two-photon absorption and the design of two-photon dyes. Angew Chem Int Ed 48(18):3244–3266
18. Beverina L, Crippa M, Salice P, Ruffo R, Ferrante C, Fortunati I, Signorini R, Mari CM, Bozio R, Facchetti A, Pagani GA (2008) Indolic squaraines as two-photon absorbing dyes in the visible region: x-ray structure, electrochemical, and nonlinear optical characterization. Chem Mater 20(10):3242–3244
19. Porrès L, Mongin O, Katan C, Charlot M, Pons T, Mertz J, Blanchard-Desce M (2004) Enhanced two-photon absorption with novel octupolar propeller-shaped fluorophores derived from triphenylamine. Org Lett 6(1):47–50
20. Segura JL, Gómez R, Martín N, Guldi DM (2001) Synthesis of photo- and electroactive stilbenoid dendrimers carrying dibutylamino peripheral groups. Org Lett 3(17):2645–2648
21. Perrin DD, Armarego WLF, Perrin DR (1966) Purification of laboratory chemicals. Pergamon, New York
22. Grabolle M, Spieles M, Lesnyak V, Gaponik N, Eychmller A, Resch-Geer U (2009) Determination of the fluorescence quantum yield of quantum dots: suitable procedures and achievable uncertainties. Anal Chem 81(15):6285–6294
23. FischerM GJ (1996) Fluorescence quantum yield of rhodamine 6G in ethanol as a function of concentration using thermal lens spectrometry. Chem Phys Lett 260(1–2):115–118
24. Maus M, Reitigg W, Bonafoux D, Lapouyade R (1999) Photoinduced intramolecular charge transfer in a series of differently twisted donor–acceptor biphenyls as revealed by fluorescence. J Phys Chem A 103(18):3388–3401
25. Lukeman M, Veal D, Wan P, Ranjit V, Munasinghe N, Corrie JE (2004) Photogeneration of 1, 5-naphthoquinone methides via excited-state (formal) intramolecular proton transfer (ESIPT) and photodehydration of 1-naphthol derivatives in aqueous solution. Can J Chem 82(14):240–253
26. Xu C, Webb WW (1996) Measurement of two-photon excitation cross sections of molecular fluorophores with data from 690 to 1050 nm. J Opt Soc Am B 13(3):481–491
27. Albota MA, Xu C, Webb WW (1998) Two-photon fluorescence excitation cross sections of biomolecular probes from 690 to 960 nm. Appl Opt 37(31):7352–7356
28. Hyperchem 8.0 Package (2002). Hyperchem Inc., Gainesville FL, USA
29. Drwar MJS, Zoebisch EG, Healy EF, Stewart JJP (1985) Development and use of quantum mechanical molecular models. 76. AM1: a new general purpose quantum mechanical molecular model. J Am Chem Soc 107(13):3902–3909
30. Mallegol T, Gmouh S, Meziane MAA, Blanchard-Desce M, Mongin O (2005) Practical and efficient synthesis of tris(4-formylphenyl)amine, a key building block in materials chemistry. Synthesis 2005(11):1771–1774
31. Chiang WY, Laane J (1994) Fluorescence spectra and torsional potential functions for trans-stilbene in its S_0 and S_1 (π, π^*) electronic states. J Chem Phys 100(12):8755–8768
32. Wang S, Kim SH (2009) Photophysical and electrochemical properties of D–π–A type solvatofluorchromic isophorone dye for pH molecular switch. Current Appl Phys 9(4):783–787
33. Albota M, Beljonne D, Brédas JL, Ehrlich JE, Fu JY, Heikal AA, Hess SE, Kogej T, Levin MD, Marder SR, McCord-Maughon D, Perry JW, Röckel H, Rumi M, Subramaniam G, Webb WW, Wu XL, Xu C (1998) Design of organic molecules with large two-photon absorption cross sections. Science 281(11):1653–1656
34. Nguyen KA, Day PN, Pachtera R (2007) Effects of solvation on one- and two-photon spectra of coumarin derivatives: a time-dependent density functional theory study. J Chem Phys 126 (9):094303–094313
35. Guo JD, Wang CK, Luo Y, Agren H (2003) Influence of electron-acceptor strength on the resonant two-photon absorption cross sections of diphenylaminofluorene-based chromophores. Phys Chem Chem Phys 5(18):3869–3873
36. He GS, Tan LS, Zheng QD, Prasad PN (2008) Multiphoton absorbing materials: molecular designs, characterizations, and applications. Chem Rev 108(4):1245–1330
37. Lippert VEZ (1957) Spektroskopische bistimmung des dipolmomentes aromatischer Verbindungen Im Ersten Angeregten Singulettzustand. Z Electrochem 61:962
38. Lakowicz JR (1999) Principles of fluorescence spectroscopy. Kluwer Academic, New York
39. Aoki K, Guo Y, Chen JY (2009) Diffusion-controlled currents in viscous solutions of polyethylene glycols. J Electroanal Chem 629 (1–2):73–77
40. Domagalska BW, Wilk KA, Wysocki S (2003) Experimental and theoretical studies on solvent effects of amphiphilic conjugated polyenals. Phys Chem Chem Phys 5(4):696–702
41. Liu J, Tu G, Zhou Q, Cheng Y, Geng Y, Wang L, Ma D, Jing X, Wang F (2006) Highly efficient green light emitting polyfluorene incorporated with 4-diphenylamino-1, 8-naphthalimide as green dopant. J Mater Chem 16(15):1431–1438
42. Bard AJ, Faulkner LA (1984) Electrochemical methods-fundamentals and applications. Wiley, New York